Journal of Membrane Science 514 (2016) 95–104

Contents lists available at ScienceDirect

Journal of Membrane Science

journal homepage: www.elsevier.com/locate/memsci

The effect of flake orientational order on the permeability of barrier membranes: numerical simulations and predictive models

Marco Dondero, J. Pablo Tomba, Adrián P. Cisilino *

Instituto de Tecnología y Ciencia de Materiales, Facultad de Ingeniería, CONICET, Universidad Nacional de Mar del Plata, Av. Juan B. Justo 4302, B7608 FDQ, Mar del Plata, Argentina

ARTICLE INFO

Article history:
Received 13 August 2015
Received in revised form
22 April 2016
Accepted 25 April 2016
Available online 26 April 2016

Keywords:
Barrier membranes
Permeability
Orientational order
Numerical simulation
Analytical model

ABSTRACT

This work presents results of numerical simulations along with the development of simple analytical forms aimed at predicting diffusivity in barrier membranes with randomly dispersed flakes. Simulations are performed using Boundary Element models of representative volume elements that account for the barrier microstructures with high level of detail. Microstructural features such as flake aspect ratio (α) and volume fraction (ϕ) are varied in the range of practical interest ($0.1 \leq \alpha\phi \leq 5$). Numerical simulations also address the effects of the flake orientational order. Simulation results are used to develop a new model that predicts the elements of the diffusivity matrix as a function of flake arrangement. The basic idea behind the proposed model is to assimilate the parameter proposed by Bharadwaj to describe flake orientational order into the diffusivity model by Lape, which was originally developed for uniformly oriented flakes. The model predictions are shown to be consistent with theoretical limiting behaviors and with those of other models in the literature. The proposed model is among the few ones that accounts for the disorder in the flake orientation, which is found to have a noticeable impact on diffusivity in the direction parallel to the flake orientation.

1. Introduction

The control of barrier properties is relevant to many technologies as a key factor to guarantee product preservation or to protect parts and objects of everyday use from the environment. Beverage bottling, food packaging, protective coatings of diverse nature or drug delivery devices are some of the many application niches that require a fine control of mass transport of gas or liquid species through the material. A useful approach to produce materials with enhanced barrier properties is the dispersion of impermeable elongated objects in a host matrix. The idea behind is that the obstacles increase the path length of the penetrating species so retarding mass transport [1]. This concept has been implemented in polymer based materials with the inclusion of elongated obstacles with lateral dimensions in the nanometric scale (polymer nano-composites). For instance, it has been shown that the incorporation of small amounts of layered silicates (clays) or natural fibers such as cellulose into a variety of polymer matrices produces a remarkable improvement in gas barrier properties.

The prediction of barrier properties like diffusivity, D, or permeability, P, in composite materials is of obvious interest, particularly from the point of view of material design. In other families of barrier materials, such as those composed by multilayers, overall permeability is dictated by a simple combination of properties of the individual layers. In nanocomposites, predictions of barrier properties are certainly more complex as there are several structural features that come into play. For instance, characteristics of the obstacles such as length-to-thickness ratio, α, volume fraction, ϕ, orientation and state of aggregation are expected to affect the overall transport behavior of the composite system. Moreover, in real materials, these variables may not have spatial homogeneity thus adding another level of complexity in the problem description. For example, in the production of parts by injection, extrusion or blown-molding of polymer nanocomposites, shear induced orientation of the nanoclay is unavoidable and it leads to fairly complex orientation patterns of the objects when going from the skin of the part to its core [2].

Some remarkable efforts have been made in the past to understand the effect of α and ϕ of either regular or randomly placed diffusion flakes on overall P or D. The upper bound for diffusivity is predicted by the Voigt's parallel model, which states that for flakes oriented parallel to the concentration gradient, diffusivity decreases, irrespectively of α, in direct proportion with the increase of ϕ. Any other configuration yields lower diffusivities; in particular, models that consider flakes oriented perpendicular to the

* Corresponding author.
E-mail address: cisilino@fi.mdp.edu.ar (A.P. Cisilino).

http://dx.doi.org/10.1016/j.memsci.2016.04.064
0376-7388/

concentration gradient predict the minimum diffusivities. These models idealize the penetrant trajectory as a one-dimensional path that experiments abrupt changes in direction when it encounters an obstacle. Thus, tortuous paths retard the penetrant diffusion. The barrier performance can be described in terms of the product $\alpha\phi$, a measure of the mean overall resistance to the diffusion of the penetrant. Models predict two ranges of barrier performance. In the *diluted* limit ($\alpha\phi \ll 1$), D scales with the inverse of the product $\alpha\phi$; obstacles essentially behave independently of each other and the reduction in diffusivity is mostly due to the tortuosity effect [3]. In the so-called *semi-diluted* regime ($\alpha\phi$ close or above 1), D turns out depending on the square inverse of $\alpha\phi$ [1]. As obstacles come closer to each other, the area available for diffusion decreases, further reducing diffusivity. The *semi-diluted* regime is of practical interest as in most of the applications $\phi \approx 0.05$ and $\alpha > 20$, which implies $\alpha\phi > 1$. Other important microstructural factors have also been considered. For instance, Lape et al. [1] assessed the influence of flake aspect-ratio polydispersity on the permeability for the case of flakes oriented perpendicular to the concentration gradient. They concluded that polydisperse flakes have superior barrier properties than monodisperse ones.

Flake orientation with respect to the concentration gradient i.e. aligned or perpendicular, have a profound effect on D. Accordingly, the dispersion of the flake orientation angles is another important aspect to be addressed, as the increase in angle dispersion eventually leads to microstructures with randomly oriented flakes. Fredrickson and Bicerano [4] demonstrated that flakes perpendicular to the concentration gradient are three times more effective in permeability reduction than those with randomly oriented obstacles. Bharadwaj [5] described the dispersion in the orientation angle (orientational order) through the introduction of the order parameter S, derived from liquid crystals theory [6]. Bharadwaj's model predicts that small obstacles are more sensitive to orientational disorder than large ones, although that claim is limited to the diluted limit used for the author as the base of derivation.

High performance numerical tools such as Boundary Element (BEM) and Finite Element (FEM) Methods have taken advantage of the continuous increases in computational power to address the rigorous modeling of complex material microstructures. BEM can solve the diffusion of the penetrant through intricate flake arrangements with high level of detail and accuracy. At the same time, BEM simplifies the problem data preparation and discretization, which is limited to the model boundary [7]. Results of numerical simulations are very useful to obtain further insights on how microstructural features such as flake size, shape and orientation influence on D, beyond the information obtained from the analysis of idealized simple microstructures. Rigorous computer simulations provide a platform of data generation, comparable to those one would obtain from experiments with controlled and well-defined sample geometries.

This work presents the results of a systematic 2D BEM homogenization analyses for the computation of the overall anisotropic diffusivity matrix of flake-filled barrier membranes. The analyses consider microstructures with randomly placed flakes, the size and aspect ratios of which are within the range $0.1 < \alpha\phi < 5$. The homogenization analyses address the effects of the variability of the flake orientation angles, which are characterized via the above referred orientational order parameter, S. Our primary objective is to reduce the simulation results to simple and manageable analytical forms, able to quantitative predict the diffusivity reductions in terms of α, ϕ and S. The paper is organized as follows: we start presenting relevant details of BEM implementation and the results of the numerical simulations. Then, we briefly review some of the relevant analytical models used to predict diffusivity, which will serve as a platform for our further developments. In the subsequent section, we develop a new analytical model that predicts the overall anisotropic diffusivity matrix of the barrier material. The last section discusses some examples that highlight the capabilities of this new model.

2. Problem description

The analysis addresses the two-dimensional diffusion of a solute through flake-filled membranes, like the ones depicted in Fig. 1. The matrix material is homogeneous and isotropic, whereas the flakes are of rectangular shape and they are impermeable to the diffusing species. Dimensions of the flakes are $2a \times b$ with $a > b$ (see Fig. 2a). The membrane microstructure is described in terms of the flake volume fraction $\phi = A_{flakes}/A_{membrane} = \frac{n(2a \times b)}{L \times W}$, where n is the number of flakes and L and W are the membrane length and width, respectively. The flake aspect ratio is defined as $\alpha = a/b$. The flake orientation is described in terms of the mean orientation angle $\bar{\theta}$ and its standard normal dispersion σ.

Fick's second law governs the diffusion of the solute through the membrane matrix. At the steady state, the conservation of the solute mass implies,

$$\nabla \bullet \mathbf{q} = 0, \tag{1}$$

where $\mathbf{q}$ is the diffusion flux. The constitutive equation for the flux is

$$\mathbf{q} = -D\nabla\varphi, \tag{2}$$

where φ is the solute concentration and D is the diffusion coefficient of the neat matrix, which is assumed to be not affected by the presence of the flakes. The symbol ∇ stands for the gradient operator. Bold letters indicate vectors and matrices. Vector components are indicated with subscripts; for instance q_1 and q_2 indicate the fluxes in the directions along and across the membrane, respectively.

Due to the presence of flakes, the membrane is anisotropic in terms of diffusion properties. The respective diffusivity matrix is

$$\mathcal{D} = \begin{bmatrix} \mathcal{D}_{11} & \mathcal{D}_{12} \\ \mathcal{D}_{21} & \mathcal{D}_{22} \end{bmatrix}, \tag{3}$$

where the $\mathcal{D}_{ij}$ components are the diffusivities associated to the flux in the i-direction due to a concentration gradient in the j-direction.

Matrix $\mathcal{D}$ is a second-order tensor, so it can be rotated using the well-known rotation formula

$$\mathcal{D}' = \mathbf{R}\mathcal{D}\mathbf{R}^T = \begin{bmatrix} \cos(\theta) & -\sin(\theta) \\ \sin(\theta) & \cos(\theta) \end{bmatrix} \begin{bmatrix} \mathcal{D}_{11} & \mathcal{D}_{12} \\ \mathcal{D}_{21} & \mathcal{D}_{22} \end{bmatrix} \begin{bmatrix} \cos(\theta) & \sin(\theta) \\ -\sin(\theta) & \cos(\theta) \end{bmatrix}, \tag{4}$$

where θ is the rotation angle.

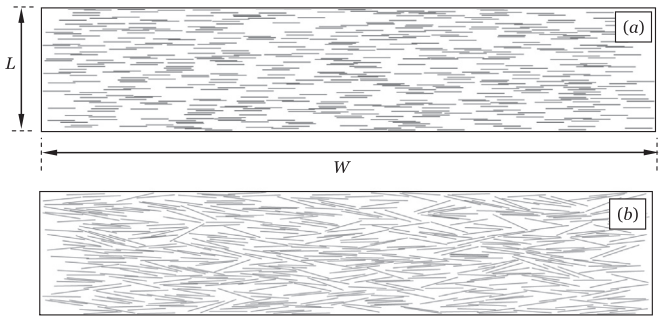

Fig. 1. Geometries of typical models of the membrane microstructures: $\phi = 0.1$, $n = 500$, $\alpha = 25$, orientation angle $\bar{\theta}$=0° with normal dispersion (a) $\sigma = 0°$ and (b) $\sigma = 10°$.

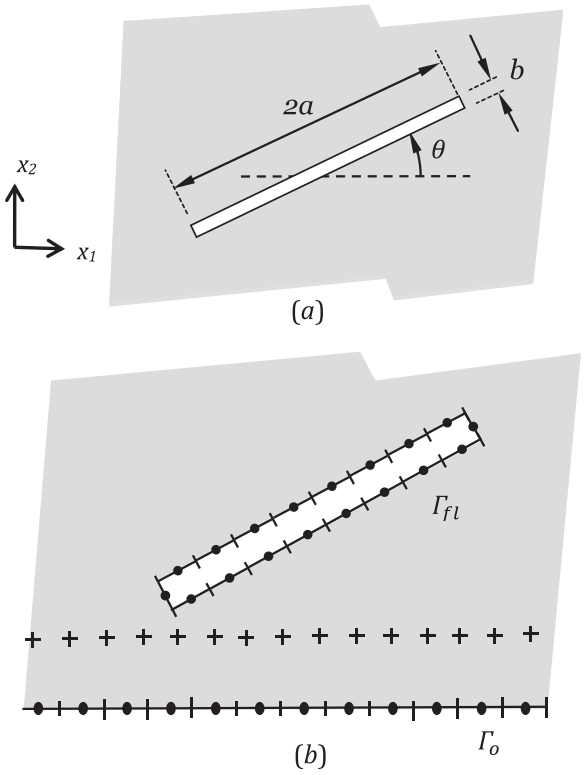

Fig. 2. BEM models of the membrane microstructure: (a) Notation for the dimensions and orientation of the flakes; (b) BEM discretization strategy: • boundary nodes, + internal points.

3. Homogenization analysis

The homogenized or effective diffusivities relate the average flux and concentration fields in the membrane. In Fig. 1, it is observed that the membrane microstructure has inhomogeneous flake distributions in the regions next to the boundaries. Since flakes are not allowed to cross the sample boundaries, flake volume fractions ϕ are smaller in the regions close to the vertical boundaries; moreover flakes placed next to the horizontal boundaries have a tendency to be oriented in parallel to the x_1-direction. Consequently, the membrane strips adjacent to the boundaries are easy diffusion zones that will lead to overestimate the membrane effective diffusivity if their contributions are directly included into the homogenization computations. Following an approach similar to that by Chen and Papathanasiou [9], the homogenization procedure used in this work excludes the strips with enhanced diffusion zones from the homogenization computations. The homogenization procedure distinguishes between two domains: i) the sample domain of area $A_0=L\times W$ and external boundary Γ_0 that comprises the complete microstructure; ii) the representative volume element (RVE) domain, of area A and external boundary Γ, which is embedded within the sample domain, see Fig. 3. The RVE is assumed large enough for the spatial fluctuations of the field variables to be statistically homogeneous [12].

For the homogenization analysis, concentration boundary conditions on the boundary Γ_0 are specified to produce average fluxes within a homogeneous material of the same size as the sample. These are

$$\bar{\varphi}(\Gamma_0) = -H_j x_j \quad j=1,2, \tag{5}$$

where $H_j=-\varphi_j$ are the given concentration gradients. The associated average flux in the RVE area is

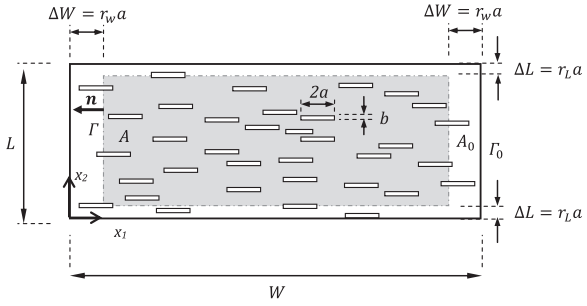

Fig. 3. Strategy for the RVE sizing: the RVE domain (gray region) embedded within the sample domain.

$$\bar{q}_i=\frac{1}{A}\int_A q_i\,dA. \tag{6}$$

A useful averaging theorem allows expressing $\bar{\boldsymbol{q}}$ in terms of a line integral along Γ [9]. Therefore, one has

$$\bar{\boldsymbol{q}}=\frac{1}{A}\int_\Gamma \boldsymbol{n}\cdot(\boldsymbol{q}\otimes\boldsymbol{x})\,d\Gamma, \tag{7}$$

where $\boldsymbol{n}$ is the unit normal vector at the boundary Γ and $\otimes$ is the dyad operator.

Similarly, the average concentration gradient $\bar{\boldsymbol{H}}$ in the RVE can be written as

$$\bar{\boldsymbol{H}}=\frac{1}{A}\int_\Gamma \varphi\cdot\boldsymbol{n}\,d\Gamma. \tag{8}$$

The method for the computation of effective properties in terms of average fields is first-order asymptotic. The average fluxes and the concentration gradients within the RVE are related by the effective diffusivity matrix, $\mathcal{D}_{ij}$, throughout the bilinear form

$$\bar{q}_i=\mathcal{D}_{ij}\bar{H}_j. \tag{9}$$

The concentration and flux fields are solved for two problems with constant concentration gradients in the x_1 and x_2 directions,

$$\mathbf{H}^1=\begin{bmatrix}-1/W\\0\end{bmatrix} \text{ and } \mathbf{H}^2=\begin{bmatrix}0\\-1/L\end{bmatrix}, \tag{10}$$

respectively. The boundary conditions for these problems are set using Eq. (5).

Finally, the effective diffusivity matrix, $\mathcal{D}$, is computed by solving the system of equations that results after the specialization of Eq. (9) for $\bar{\mathbf{q}}^1$ and $\bar{\mathbf{H}}^1$, and $\bar{\mathbf{q}}^2$ and $\bar{\mathbf{H}}^2$. Thus,

$$\mathcal{D}=\begin{bmatrix}-\bar{q}_1^1/\bar{H}_1^1 & -\bar{q}_1^2/\bar{H}_2^2\\ -\bar{q}_2^1/\bar{H}_1^1 & -\bar{q}_2^2/\bar{H}_2^2\end{bmatrix}. \tag{11}$$

4. Numerical implementation

4.1. Boundary element modeling

This work uses the Fast Multipole formulation of the BEM (FMBEM) to solve the flux and concentration fields for the homogenization analyses. The FMBEM reduces the computational cost of the direct BEM from an order of $O(N^3)$ to a quasi-linear, where N is the number of degrees of freedom of the problem. This reduction is achieved by: i) multilevel clustering of the boundary elements into cells along with the use of the multipole series expansion for the evaluation of the fundamental solutions in the far field; ii) the use of an efficient iterative solver. Additionally, the multipole algorithm leads to important savings in computer

memory as it involves a matrix-free calculation scheme [8].

In the BEM model, the flakes are assimilated to rectangular holes with zero-flux boundary condition along their boundaries, Γ_{fl}, like in Chen and Papathanasiou [9] and Dondero et al. [10,20]. The outer model boundary, Γ_0, and the flake boundaries, Γ_{fl}, are discretized with constant elements of size equal to that of the flake thickness (see Fig. 2b). This discretization strategy was devised based on the results of convergence tests performed in previous works, see Ref. [10,11].

The FMBEM was implemented in-house, following the tutorial due to Liu and Nishimura [8]. Integral evaluations are carried out analytically. The system of equations is solved by a preconditioned GMRES algorithm from the Slatec public library, available at netlib (http://www.netlib.org/). The parameters of the algorithm were set as follows: 12 expansion terms for the FMBEM and 300 elements per cell. The tolerance for the GMRES convergence was set 10^{-7}. With these settings, the speedup of the FMBEM with respect to a standard direct BEM was around $14\times$ for 10^4-element models.

Given a membrane microstructure, FMBEM models are solved for the boundary conditions in (10). In the post processing stage, M internal points are used to define the contour of the RVE, see Fig. 2b and Fig. 3. Distances between internal points are set equal to half the element size in order to capture the rapid varying fields in the proximity of the flakes. Fluxes and concentrations are computed at internal points using standard BEM procedures. These results are then used to compute the RVE average flux and concentration gradients by means of the discrete versions of Eqs. (7) and (8), assuming a piecewise constant interpolations of the flux and concentration fields along the contour Γ. Thus,

$$\bar{\boldsymbol{q}}=\frac{1}{A}\sum_{k=1}^{M}\boldsymbol{n_k}\bullet(\boldsymbol{q_k}\otimes\boldsymbol{x_k})\delta\boldsymbol{\Gamma} \tag{12}$$

and

$$\bar{\boldsymbol{H}}=\frac{1}{\boldsymbol{A}}\sum_{k=1}^{M}\varphi_k\bullet\boldsymbol{n_k}\delta\boldsymbol{\Gamma}, \tag{13}$$

where $\boldsymbol{n_i}$, $\boldsymbol{q_i}$, φ_i and $\boldsymbol{x_i}$ are the normal vector, the flux and the concentration at the position of the k^{th} internal point and $\delta\boldsymbol{\Gamma}$ is distance between internal points. Finally, the results for $\bar{\mathbf{q}}^1=\left[\bar{q}_1^1\ \ \bar{q}_2^1\right]^T$, $\bar{\mathbf{q}}^2=\left[\bar{q}_1^2\ \ \bar{q}_2^2\right]^T$, $\bar{\mathbf{H}}^1=\left[\bar{H}_1^1\ \ \bar{H}_2^1\right]^T$ and $\bar{\mathbf{H}}^2=\left[\bar{H}_1^2\ \ \bar{H}_2^2\right]^T$.

are replaced into (11) to compute the effective diffusivity matrix $\mathcal{D}$.

4.2. RVE sizing

The strategy for the RVE sizing is depicted in Fig. 3. It consists in determining the number of flakes, n, the sample aspect ratio, W/L, and the width of the excluded boundary strips, $\Delta W = r_w a$ and $\Delta L = r_L a$, that result in size-independent diffusivity properties for the RVE. This was done by means of convergence analyses for successive larger samples and by increasing values for the parameters r_w and r_L.

Multiple criteria were devised and tested. The resultant one is illustrated and discussed next for the microstructure shown in Fig. 1a, which has flake volume fraction $\phi = 0.1$, flake aspect ratio $\alpha = 25$ and monodisperse flake orientation angle $\theta = 0°$. This is a very good exemplary case because, being in the concentrated regime ($\alpha\phi = 2.5$), the effects of the excluded zones are significant. Besides, other authors have solved this case and so their results can be used to verify our results.

Fig. 4 presents the results of the convergence analyses for the RVE flake volume fraction and the normalized concentration gradient as functions of the sample size for r_w=2 and r_L=0. 5. Every

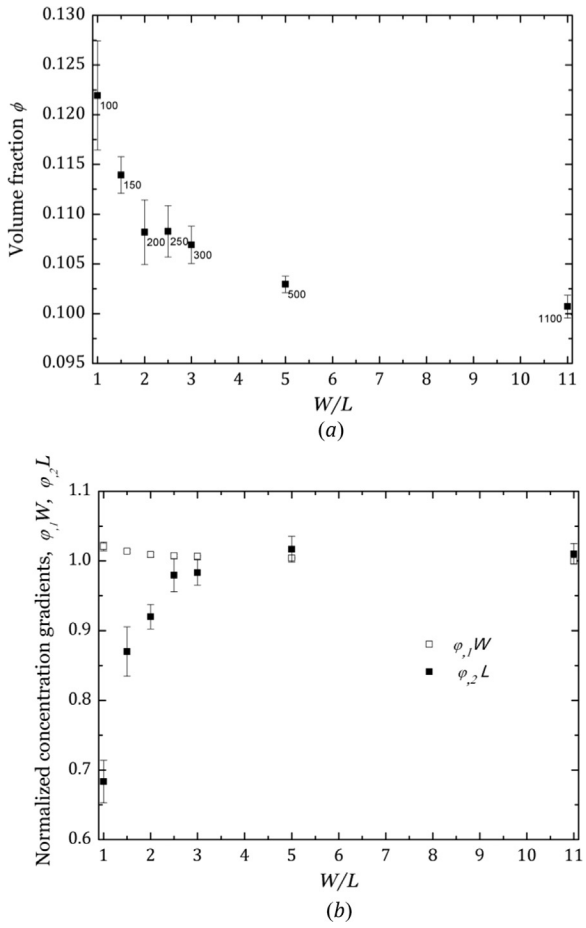

Fig. 4. Convergence analyses for the RVE (a) flake volume fraction and (b) normalized concentration gradient as functions of the normalized sample size for r_w=2 and r_L=0. 5. Error bars indicate standard deviations. Point labels in (a) indicate the number of flakes in the sample.

point in the plots is the average of 10 results computed for different random microstructures. Error bars indicate standard deviations. Point labels in Fig. 4a indicate the number of flakes in the samples. BEM discretizations range from 32,000 to 118,000 elements.

The variation of the RVE flake volume fraction ϕ with the sample size in Fig. 4a is due to the effect of excluding the boundary strips. Since the strips have less flakes than the central part, ϕ in the RVE is larger than the nominal value used to generate the sample microstructure. As it is expected, ϕ converges towards the nominal value as the sample size increases and the area of the excluded strips covers a smaller fraction of the sample area; the mean value of the discrepancy between the RVE and the sample (nominal) flake volume fractions diminishes from 22% for W/L=1 (100 flakes) to 3% for W/L=5 (500 flakes) and to less than 1% for W/L=11 (1100 flakes). In the same way, the standard deviation for ϕ diminishes with sample size, from approximately 4–1% over the analysis range. Similar results were obtained for microstructures with $0.02 \le \phi \le 0.1$, flake aspect ratios $5 \le \alpha \le 50$ and orientation angles with a normal variability up to $\sigma = 20°$. For W/L=5, the discrepancy in ϕ never exceeded 5% and the dispersions for ϕ were always less than 2%. It is worth to mention that although the consistent overestimation of ϕ, RVEs and their associated results will be always identified in the text by their nominal ϕ. However, all the computations and plots will be produced using the actual ϕ values.

Fig. 4b plots the effect of the sample size on the RVE concentration gradients, $\varphi_{,1}$ and $\varphi_{,2}$. Concentration gradient results are

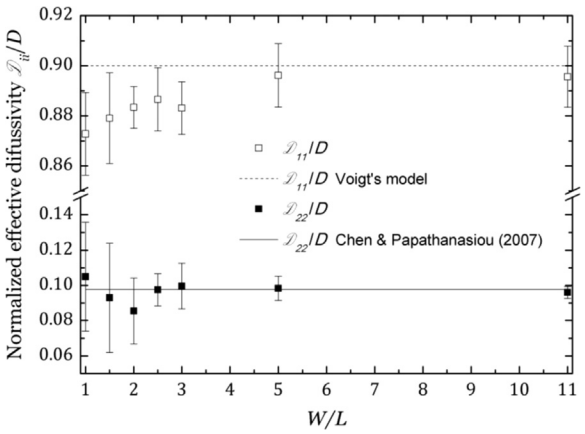

Fig. 5. Convergence analyses for the effective diffusivities $\mathcal{D}_{11}$and $\mathcal{D}_{22}$ as functions of the normalized sample size for r_W=2 and r_L=0. 5.

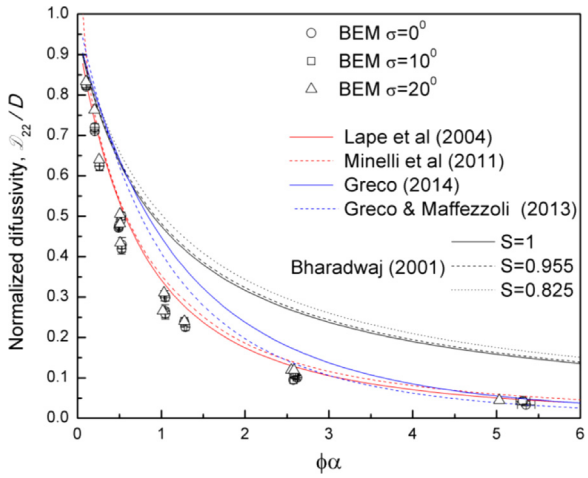

Fig. 6. BEM and analytical-model results for diffusivity $\mathcal{D}_{22}$ for flakes with average orientation $\bar{\theta}$=0°.

normalized with respect to the values for the boundary conditions in Eq. (10). It can be observed that both concentration gradients converge towards their prescribed values. Gradient φ_1 is less sensitive to the sample size than φ_2. Even for the smallest sample size, W/L=1, φ_1 presents a deviation less than 2%, which reduces to less than 0.5% for W/L>5. On the other hand, the discrepancy of φ_2 reduces from around 30% for W/L=1 to less than 2% for W/L>5. Standard deviations of φ_1 are negligible over the complete range of sample sizes, whereas those for φ_2 reduces from 6% to less than 2%. The analysis of other microstructures led to similar results. In every case, the same levels of accuracy were found for the mean values of φ_j, but standard deviations were larger for microstructures with high aspect ratios and orientational order. Standard deviations for microstructures with $\alpha = 50$ and $\sigma = 20^\circ$ were found to be as large as 12% for W/L=5.

Finally, the results for the convergence of the effective diffusivity are presented in Fig. 5. There are also plot in the figure the reference values for the Voigt's (parallel) model [18] for comparison with the $\mathcal{D}_{11}$ computations,

$$\frac{\mathcal{D}_{11}}{D}=1-\phi=1-0.1=0.9, \tag{14}$$

and the numerical result by Chen and Papathanasiou [9], $\mathcal{D}_{22}/D$=0.09766, for comparison with the $\mathcal{D}_{22}$ computations. It can be observed that both, $\mathcal{D}_{11}$and $\mathcal{D}_{22}$, converge to the reference values. For $W/L\geq5$, $\mathcal{D}_{11}$ matches that of Voigt's model with a discrepancy less than 0.5%, whereas the difference between $\mathcal{D}_{22}$ and the results by Chen and Papathanasiou [9] is within 1.5%. Standard deviations are 1.5% for $\mathcal{D}_{11}$ and less than 5% for $\mathcal{D}_{22}$. The analyses of the diffusivities for other microstructures showed similar behaviors, but, as it was reported before for the concentration gradient, standard deviations increase for microstructures with high aspect ratios and orientational order. Standard deviations for microstructures with $\alpha = 50$ and $\sigma = 20^\circ$ were found to be as large as 15%.

Based on the above results, and considering a balance between accuracy and computational cost, the RVE size is designed to contain 500 flakes, aspect ratio W/L=5 and excluded strips of width $\Delta W = 2a$ and $\Delta L = 0.5a$.

5. BEM results

The above procedures were used to study the effects of the flake volume fraction, aspect ratio and orientational order on the membrane effective diffusivity. BEM models were solved for combinations of ϕ = [0.02,0.05,0.1] and α = [5,10,25,50]. Three cases were considered for the orientational order, σ = [0°,10°, 20°]. The average flake orientation was always $\bar{\theta}$=0°. That made a total of 36 different analysis cases. Those with $\sigma = 0^\circ$ and 10° were solved for 10 different RVEs; a single one was solved for $\sigma = 20^\circ$. RVEs were generated randomly, by successive addition of non-overlapping flakes with uniform probability distribution for the position and normal (Gaussian) distribution for the orientation angle [13]. The resultant diffusivity matrices are labeled as $\mathcal{D}^{\sigma 0}$, $\mathcal{D}^{\sigma 10}$ and $\mathcal{D}^{\sigma 20}$.

Fig. 6 depicts the results for the normalized $\mathcal{D}_{22}/D$ in terms of $\phi\alpha$ for the three values of σ. Symbols correspond to BEM results whereas lines represent predictions of analytical models that will be discussed in the next section. Error bars, hidden behind the symbols in most of the cases, indicate the normal dispersion of the BEM results. Dispersion in abscissas are due to the variations of ϕ (see Section 4.2). It can be observed that the three sets of results have same general behavior. As it was expected, diffusivity across the membrane decreases with the increments of flake volume fraction and aspect ratio. Besides, orientational disorder has a weak effect, only producing small increments in diffusivity.

Fig. 7 shows results for $\mathcal{D}_{11}/D$; BEM results are represented by symbols whereas lines correspond to model predictions that will be discussed later. It is observed that results for $\sigma = 0$ converge towards the Voigt's limit value, $\mathcal{D}_{11}/D=1-\phi$, as flake aspect ratios increase. On the other hand, flake misalignments (σ=10° and σ=20°) lead to reductions in the diffusivity; this effect is more marked as flake volume fraction, aspect ratio and dispersion in the orientation increase. Before further discussing on the results, it is important to comment on the orientational disorder of the microstructures. Geometrical restrictions imposed by the condition of not overlapping flakes yield samples with values of normal dispersions in flake orientation that are smaller than the target value. This effect is more marked with the increment of the flake volume fraction and aspect ratio, as the flakes need to be "more ordered" to attain the prescribed volume fractions. Results computed using samples with normal dispersions in the flake orientation angles that deviate more than 15% from their target values are marked with circles in Fig. 7. For instance, the actual dispersion for the data point labeled $\phi = 0.05$, $\alpha = 50$ and $\sigma = 20^\circ$ in Fig. 7b is $\sigma = 16.8^\circ$; while in Fig. 7c, the actual dispersion values are $\sigma = 16.5^\circ$, 15.6° and 13.5° for α = 10,25 and 50, respectively. This behavior shows the practical threshold for the random disorientation of the flakes.

We can quantify the reduction of $\mathcal{D}_{11}$ due to the orientational disorder from the results in Fig. 7. For example, for $\phi = 0.02$ and

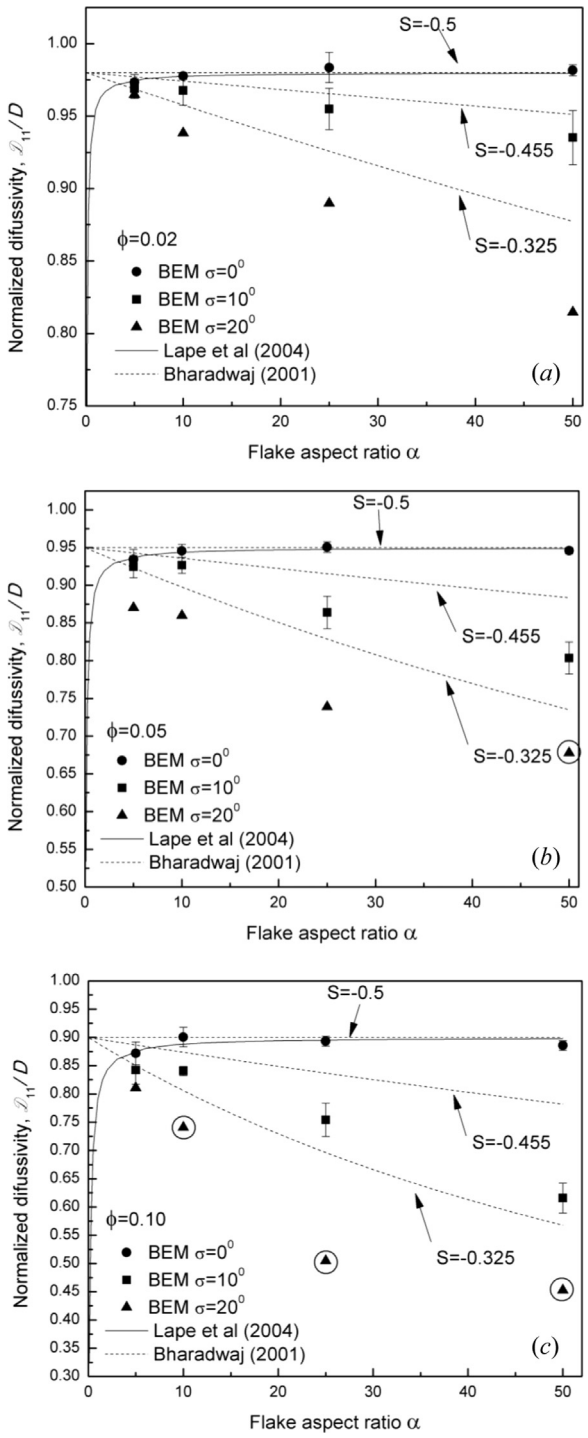

Fig. 7. BEM results for $\mathcal{D}_{11}$ for flakes oriented $\bar{\theta}$=0°: (a) ϕ = 0.02, (b) ϕ = 0.05 and (c) ϕ = 0.1.

α = 50, the reduction in the diffusivity with respect to the case of perfectly oriented flakes are $\mathcal{D}_{11}^{\sigma 10}/\mathcal{D}_{11}^{\sigma 0}$=0.95 and $\mathcal{D}_{11}^{\sigma 20}/\mathcal{D}_{11}^{\sigma 0}$=0.90, while for ϕ = 0.05 they are $\mathcal{D}_{11}^{\sigma 10}/\mathcal{D}_{11}^{\sigma 0}$=0.91 and $\mathcal{D}_{11}^{\sigma 20}/D\approx$0.72. For ϕ = 0.1 the reduction in the diffusivity is $\mathcal{D}_{11}^{\sigma 10}/\mathcal{D}_{11}^{\sigma 0}$=0.70 and $\mathcal{D}_{11}^{\sigma 20}/\mathcal{D}_{11}^{\sigma 0}\approx$0.5. Values reported as approximated are expected to be lower, as they resulted from models with σ values lower than those nominally prescribed.

In terms of cross-diffusivities, $\mathcal{D}_{ij}$,BEM results yielded values of $\mathcal{D}_{12}$ and $\mathcal{D}_{21}$ that were, at most, about 1% of those for $\mathcal{D}_{11}$. Therefore, $\mathcal{D}_{12}$=$\mathcal{D}_{21}$=0 are assumed for all the cases.

6. Models for the prediction of the diffusivity of flake-filled membranes

This section reviews some models for the prediction of the diffusivity of the flake-filled membranes. The review does not attempt to be exhaustive, but it focuses on those approaches that will be used later for the development of the new model.

Most of the models are focused on the prediction of diffusivity across membranes with flakes oriented in the direction perpendicular to the concentration gradient, the configuration that maximizes the barrier effect. Among these models, there are those proposed by Lape et al. [1] and Minelli et al. [14]. Lape's [1] model accounts for two effects resulting from impermeable flakes replacing the permeable matrix material: the increment in the tortuosity of the diffusion path and the reduction of the area available for diffusion. As result, the reduction in diffusivity is given in terms of α and ϕ as follows:

$$\left(\frac{\mathcal{D}_{22}}{D}\right)_{\text{Lape}}=\frac{1-\phi}{\left(1+\frac{2}{3}\alpha\phi\right)^2}. \tag{15}$$

The model by Minelli is based on the fundamental work by Aris [15], to assess the effects of tortuosity, and on FEM results, to assess the resistance of the solute to pass through the gaps between flakes. The model distinguishes between two regimes, which are fully described in terms of α and ϕ:

$$\left(\frac{\mathcal{D}_{22}}{D}\right)_{Minelli} = \begin{cases} r \le \left(1\frac{\phi}{2\alpha}(\alpha+2)^2+\frac{\phi^2(\alpha+2)^4}{4\left[\alpha^2-\alpha\phi(\alpha+2)\right]}+\frac{2\phi}{\pi\alpha}(\alpha+2)^2 \ln\left[\frac{2}{\pi}\left(\frac{\alpha}{\phi(\alpha+2)}-1\right)\right]\right)^{-1} \\ r > 1\left(1+\frac{\phi}{2}(\alpha+2)+\frac{2\phi}{\pi\alpha}(\alpha+2)^2 \ln\left[\frac{1}{\pi}(\alpha+2)\right]\right)^{-1} \end{cases}$$

$$\text{where } r=\frac{2(\alpha-\phi(\alpha+2))}{\phi(\alpha+2)^2}. \tag{16}$$

Among the great number of available models, the only ones that account for the effect of flake orientation are those by Bharadwaj [5], Greco and Maffezzoli [16] and Greco [17]. Bhardwaj's model strives to predict the diffusivity strictly based on tortuosity arguments. It invokes the pioneer model by Nielsen [3] for regularly spaced flakes, which is modified to consider the dependence of the tortuosity factor with the flake orientational order via the parameter

$$S=\frac{1}{2}\langle 3\cos^2\theta-1\rangle. \tag{17}$$

The angular brackets in (17) denote averaging over all the flakes in the system. The order parameter ranges from S = 1 for θ = 0, this is, all the flakes are perfectly oriented in the membrane longitudinal direction, to S = −1/2 for θ = 90°, this is, all the flakes are perfectly oriented in the direction of the membrane thickness. The value S = 0 indicates a random orientation of the flakes. The reader is referred to Fisch and Kumar [6] for the details on the definition of S. The expression of Bharadwaj's model is given by

$$\left(\frac{\mathcal{D}_{22}}{D}\right)_{\text{Bharadwaj}}=\frac{1-\phi}{1+\frac{2}{3}\alpha\phi\left(S+\frac{1}{2}\right)}. \tag{18}$$

It is worthwhile emphasizing here that Bharadwaj's model does not aim to account for the effects of the mean flake orientation angle, $\bar{\theta}$, but for effects of their orientational order. The mean

orientation angle in Bharadwaj's model is always $\bar{\theta}=0$.

By contrast, the models by Greco and Maffezzoli [16] and Greco [17] aim to predict the effect of the overall mean flake orientation, which is given by the θ angle, assumed to be the same for all the flakes. These models were derived from the probability of collision of diffusing particles on the flakes. The expressions for the models by Greco and Maffezzoli [16] and Greco [17] are

$$\left(\frac{\mathcal{D}_{22}}{D}\right)_{\text{Greco \&Maffizzoli}}=\left(1+\frac{\pi}{\sqrt{3}}\frac{\phi}{3.62}\frac{\alpha}{2}\cos\theta(1-\sin\theta)\right)^{-4} \tag{19}$$

and

$$\left(\frac{\mathcal{D}_{22}}{D}\right)_{\text{Greco}}=\frac{1-\phi}{\left[1+\sqrt{2}\left(1-\frac{\sqrt{2}}{2}\right)\phi\frac{\alpha}{2}\cos^2\theta\right]^4}, \tag{20}$$

respectively.

Fig. 6 compares the BEM and model predictions for $\mathcal{D}_{22}/D$. It is found that models by Lape and Minelli are those that better predict the general behavior of BEM results over the complete range of $\phi\alpha$. Lape's and Minelli's predictions deviate 4% from the BEM results for $\sigma=0^\circ$ in the dilute regime, this is $\phi\alpha\lesssim 0.25$. Maximum deviations are for the concentrated regime, $\phi\alpha\gtrsim 5$, with differences of around 30% and 80% with respect to the BEM results for Lape's and Minelli's models, respectively. Models by Greco and Maffezzoli and by Greco behave similarly to those of Lape or Minelli for dilute and concentrated regimes, but they have worse performances in the medium $\phi\alpha$-range. Differences between Greco's model predictions and BEM results nearly triple those of Lape's and Minelli's models for $\phi\alpha\approx 1.3$.

For the evaluation of Bharadwaj's model, we propose to express the order parameter (17) in terms of the flake orientation dispersion σ as follows

$$S=S_{22}=\frac{1}{2}(3\cdot\cos^2\sigma-1), \tag{21}$$

such that $S=1$ for $\sigma=0^\circ$, $S=0.955$ for $\sigma=10^\circ$ and $S=0.825$ for $\sigma=20^\circ$. It is worth to note that values for S computed using (21) differ less than 1% with respect to those computed using (17) for the individual flakes.

From Fig. 6, we observe that Bharadwaj's model presents a good agreement with BEM results in the dilute regime, but it consistently draws away from those as $\phi\alpha$ increases. Discrepancies between Bharadwaj's predictions and BEM results can be as large as 300% in the concentrated regime. Although this poor performance in the concentrated regime, Bharadwaj's model shows the capability to assess the effect of the orientational order on the diffusivity. Note from Fig. 6 that increments in diffusivity predicted by Bharadwaj's model are of the same relative magnitude of those predicted by the BEM analyses.

We now address the comparison between the BEM results and the model predictions for $\mathcal{D}_{11}/D$. Lape's model [1] can be adapted to compute $\mathcal{D}_{11}/D$ by simply substituting α by its reciprocal in (15):

$$\left(\frac{\mathcal{D}_{11}}{D}\right)_{\text{Lape}}=\frac{1-\phi}{\left(1+\frac{2}{3}\frac{\phi}{\alpha}\right)^2}. \tag{22}$$

It is interesting to note the limiting behaviors of expression (22). Diffusivity values predicted by (22) converges to Voigt's limiting values for $\alpha\to\infty$, whereas they rapidly diminish as $\alpha\to 0$. This last result is consistent with the fact that as $\alpha\to 0$ the flake dimension $b\gg a$, and so, the barrier effect in the membrane longitudinal direction increases. In this condition, the problem can be tackled using Lape's model in (15) for the membrane rotated 90°. Lape's model predictions are compared to BEM results for $\sigma=0^\circ$ in Fig. 7. An excellent agreement is observed between the two sets of results, with Lape's predictions always lying within the normal dispersion of the BEM results, even for small values of α.

On the other hand, Minelli's model [14] cannot be easily adapted to compute $\mathcal{D}_{11}/D$. The simple substitution of α by its reciprocal in (16) in not possible as with the Lape's model. Due to its complex formulation, Minelli's model requires a deeper analysis to be adapted or extended for the computation of $\mathcal{D}_{11}/D$.

The computations of $\mathcal{D}_{11}/D$ by means of the models by Greco and Maffezzoli and Greco are straightforward as they only require for the specialization of (Eqs. (19) and 20), respectively, for $\theta=90^\circ$. Greco and Maffezzoli's [16] model is problematic since it violates the bound due to the Voigt's parallel model; note that Eq. (19) with $\theta=90^\circ$ predicts $\mathcal{D}_{11}/D=1$ irrespectively of ϕ and α. On the other hand, Eq. (20) of Greco's model reduces to Voigt's parallel model, which is a function of ϕ only.

To compute $\mathcal{D}_{11}/D$ with Bharadwaj's [5] model, the definition of the order parameter in (21) is adapted to make the orientation dispersion compatible with the mean flake orientation:

$$S=S_{11}=\frac{1}{2}\left[3\cdot\cos^2(\sigma+90^\circ)-1\right]; \tag{23}$$

such that $S=-0.5$ for $\sigma=0$, $S=-0.455$ for $\sigma=10^\circ$ and $S=-0.325$ for $\sigma=20^\circ$. Bharadwaj's model predictions are shown in Fig. 7. Note that Bharadwaj's model reduces to the Voigt's parallel model for $S=-0.5$, this is, it predicts constant diffusivity values irrespectively of α, and so, it overestimates diffusivities for small flake aspect ratios. On the other hand, Bharadwaj's model is successful to account for the decrements in the diffusivity due to the orientational disorder; nevertheless, its predictions result in consistent overestimations of BEM results. Discrepancies between BEM results and model predictions increase with α, ϕ and S. For $\phi=0.02$, $\alpha=50$ and $S=-0.455$ the discrepancy is only 2%, but it increases up to around 70% for $\phi=0.1$, $\alpha=50$ and $S=-0.325$.

7. A new model for the prediction of the diffusivity tensor

It is introduced here a new model for the prediction of the full diffusivity tensor in terms of flake volume fraction, aspect ratio and orientational order. The new model combines the models by Lape et al. and Bharadwaj, which are conveniently adjusted and adapted for consistency, while seeking to maintain the simplicity of the equations.

It has been shown in the previous section that Lape's model provides the best predictions for D_{11} and D_{22} when flakes are oriented with $\theta=0^\circ$ and $\sigma=0^\circ$. At the same time, Bharadwaj's model is the only one that accounts for the effects of the flake orientational order. This motivates to use Bharadwaj's approach to extend Lape's model to account the effect of the orientational disorder in a more general approach. To this end, we retrieve Eq. (15) and we modify its denominator to make it function of the order parameter S. This results in

$$\left(\frac{\mathcal{D}_{22}}{D}\right)=\frac{1-\phi}{\left[1+\frac{2}{3}\alpha\phi\frac{2}{3}\left(S+\frac{1}{2}\right)\right]^2}. \tag{24}$$

Note that the above expression reduces to Lape's model in (15) when $S=1$, and, like Bharadwaj's model, it converges to the Voigt's parallel model when $S=-0.5$.

Consistently with Lape's model, $\mathcal{D}_{22}/D$ predictions by Eq. (24) can deviate up to 30% from the numerical results, see Section 5. In order to improve this performance, we introduce an empirical correction to (24) that consists in adding a coefficient C to the second summand in its denominator:

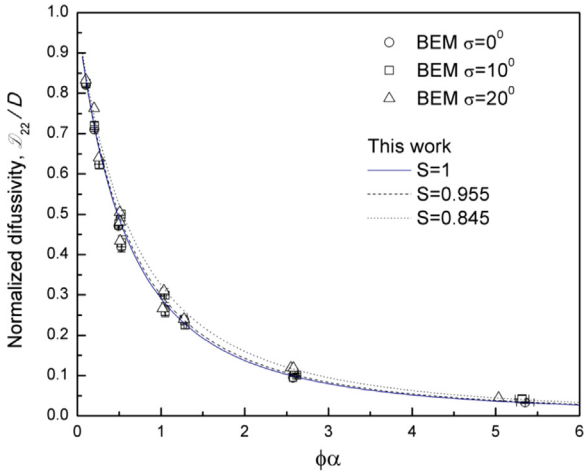

Fig. 8. Comparison of the model predictions and BEM results for D_{22}.

$$\left(\frac{\mathcal{D}_{22}}{D}\right)=\frac{1-\phi}{\left[1+C\frac{2}{3}\alpha\phi\frac{2}{3}\left(S+\frac{1}{2}\right)\right]^2}. \tag{25}$$

The coefficient C is calculated to best fit of the BEM results for $S=1$, which yields $C=5/4$. The coefficient C can be assimilated to an empirical 25% increment to the first of 2/3-factors in (25), which accounts for the effect of the random distribution of flakes in Lape's tortuosity model [1]. Then, the resultant expression for the estimation of $\mathcal{D}_{22}/D$ is

$$\left(\frac{\mathcal{D}_{22}}{D}\right)=\frac{1-\phi}{\left[1+\frac{5}{9}\alpha\phi\left(S+\frac{1}{2}\right)\right]^2}. \tag{26}$$

Fig. 8 compares the predictions by Eq. (26) to BEM results. A very good agreement between the two sets of results can be observed. Model predictions deviate less than 5% from BEM results in the dilute and intermediate regimes. Maximum discrepancies are in the concentrated regime, with differences of up to 12% for $\phi\alpha\gtrsim 2$.

Like Bharadwaj's model in Section 5, Eq. (26) can be used to compute $\mathcal{D}_{11}/D$ when S is calculated using Eq. (23). The results are plot in Fig. 9 using dashed lines. When compared to results in Fig. 7, it can be observed that the performance of the new model improves with respect to those of Bharadwaj's [5]. Discrepancies for $\phi=0.02$ do not exceed 1%, while for $\phi=0.05$ the maximum discrepancy is 7% for $S=-0.455$ and $\alpha=50$. For $\phi=0.1$, the discrepancies are more important. The maximum difference for $S=-0.455$ is 14%. Discrepancies of about 15% are found for $S=-0.325$; however, it is worth to remember that BEM results for this last case are not accurate, being , most likely, underestimated (see Section 4).

Fig. 9 shows that, consistently with Bharadwaj's model, Eq. (26) reduces to the Voigt's parallel model when specialized for $S=-0.5$, therefore, it predicts constant $\mathcal{D}_{11}/D$ values irrespectively of the flake aspect ratios. It might be desirable for the model to account for the decrease in diffusivity for low aspect ratios, as Lape's model does. To this end, the following expression is proposed for the computation of $\mathcal{D}_{11}/D$, which combines Lape's model in (22) with the denominator of expression (26):

$$\left(\frac{\mathcal{D}_{11}}{D}\right)=\frac{\frac{1-\phi}{\left(1+\frac{2}{3}\frac{\phi}{\alpha}\right)^2}}{\left[1+\frac{5}{9}\alpha\phi\left(S+\frac{1}{2}\right)\right]^2}. \tag{27}$$

The above expression yields the Lape's model in (22) when $S=-0.5$ and the Voigt's parallel model for $\alpha\to\infty$.

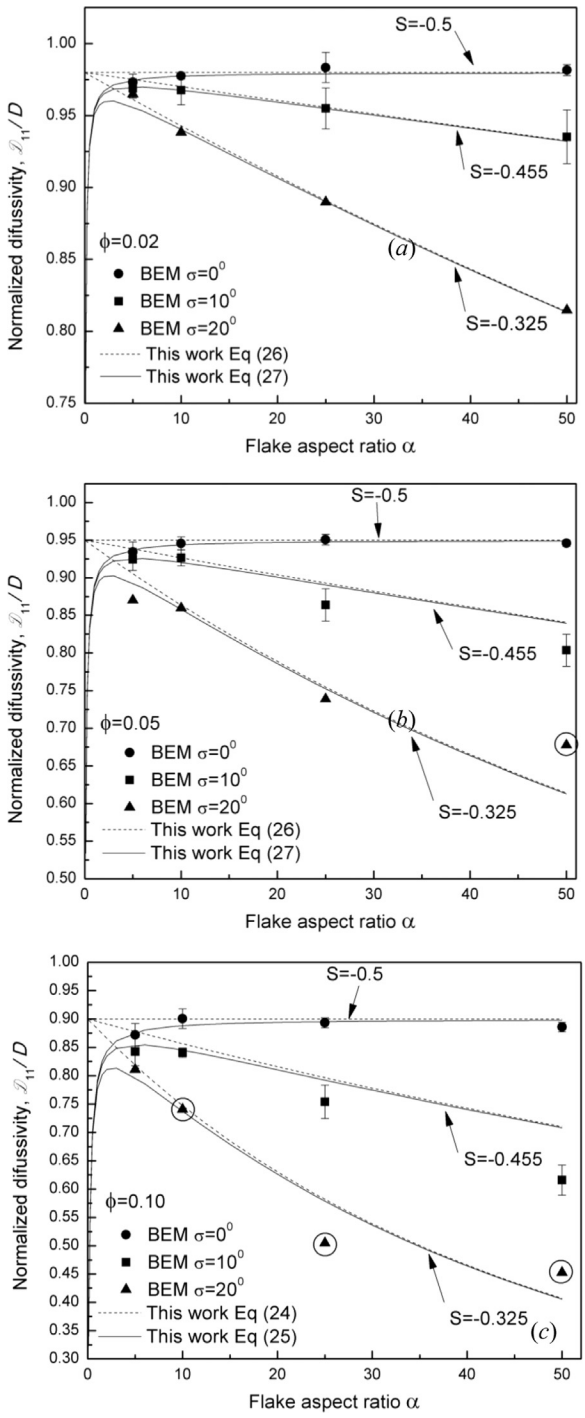

Fig. 9. Model and BEM results for D_{11}: (a) $\phi=0.02$, (b) $\phi=0.05$ and (c) $\phi=0.10$.

The predictions computed with (27) are plot in Fig. 9 using solid lines. It is observed that the improved model succeeds in accounting for the decrease in the diffusivity for low flake aspect ratios, whereas it behaves as the model described by (26) for high aspect ratios.

8. Discussion

The new model in the previous section introduces two approaches for the computation of diffusivities in the longitudinal and through-the-thickness membrane directions. The first

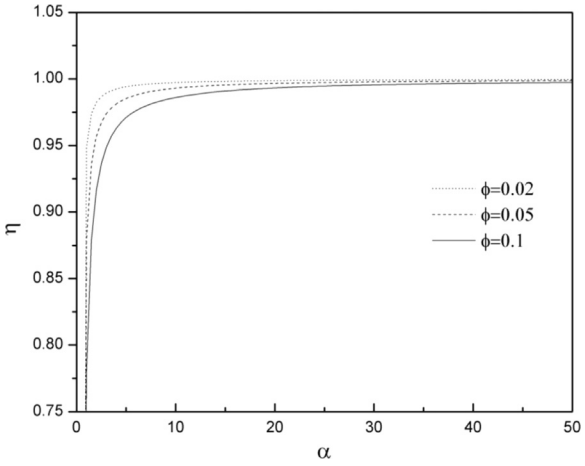

Fig. 10. Consistency between the model predictions for randomly oriented microstructures, as calculated from Eq. (26) for $\mathcal{D}_{22}/D$ and Eq. (27) for $\mathcal{D}_{11}/D$. η is defined as $\mathcal{D}_{11}^{S=0}/\mathcal{D}_{22}^{S=0}$.

approach uses a single expression, Eq. (26), to compute both diffusivities; consequently, the model has a continuous behavior over the complete S-range. The second approach uses two expressions: Eq. (26) for the computation of $\mathcal{D}_{22}/D$ and Eq. (27) for the computation of $\mathcal{D}_{11}/D$, which is better suited to deal with low aspect-ratio flakes.

In what follows we check the consistency between Eqs. (26) and (27), which should produce identical predictions for randomly oriented high aspect-ratio flakes. To predict diffusivities for randomly oriented flakes we make S=0 in Eq. (26) to compute $\mathcal{D}_{22}^{S=0}$, and in Eq. (27) to compute $\mathcal{D}_{11}^{S=0}$. In Fig. 10, we compare the two results by plotting the ratio $\eta = \mathcal{D}_{11}^{S=0}/\mathcal{D}_{22}^{S=0}$ as a function of α for different values of ϕ. It is observed that $\eta < 1$, this is, diffusivities predicted by Eq. (26) are consistently larger than those predicted by Eq. (27). For low aspect-ratio flakes, the difference between the two predictions augments markedly with the increase of ϕ. On the other hand, the two equations show the desired consistent behavior for large aspect-ratio flakes, as $\eta \to 1$ when α increases. For $\alpha > 10$, the two predictions differ by less than 1% for $\phi \leq 0.05$ and by less than 2.5% for $\phi \leq 0.1$. For $\alpha > 50$, they differ by less than 0.1% irrespectively of ϕ.

A second consistency test is the comparison with the analytical result by Fredrickson and Bicerano [4], which states that the ratio

$$\chi = \frac{1 - D/\mathcal{D}_{22}^{S=0}}{1 - D/\mathcal{D}_{22}^{S=1}} \tag{28}$$

should asymptotically approach $\chi = 1/3$ as $\phi\alpha \to 0$ for high aspect-ratio flakes.

We evaluate the numerator of (28) following two approaches: using $\mathcal{D}_{22}^{S=0}$ from Eq. (26) and using $\mathcal{D}_{11}^{S=0}$ from Eq. (27). Like in Lusti et al. [19], we check the limit behavior of (28) empirically, by plotting χ as a function of $\alpha \to \infty$ for values of $\phi \to 0$. Fig. 11 shows the two sets of results, which are labeled χ_{11} and χ_{22} for $\mathcal{D}_{11}^{S=0}$ and $\mathcal{D}_{22}^{S=0}$, respectively. It can be observed that both curves behave accordingly with the theoretical limit; for example, for $\phi\alpha = 0.001$ and $\alpha = 1000$ they deviate less than 0.1% from the theoretical value of 1/3.

We show next the use of the model to estimate the diffusivity of membrane with arbitrarily oriented flakes. Let's say that we have a membrane with $\phi = 0.03$, $\alpha = 50$, and flakes oriented with mean angle $\bar{\theta}$=25° with normal dispersion $\sigma = 20°$. We first compute $\mathcal{D}_{22}^{\sigma=20°}$ and $\mathcal{D}_{11}^{\sigma=20°}$ using Eqs. (26) and (27) with the order parameters associated to the normal dispersions around $\theta = 0°$ and $\theta = 90°$, respectively. These are S_{22}=0.825 and S_{11}= − 0.325.

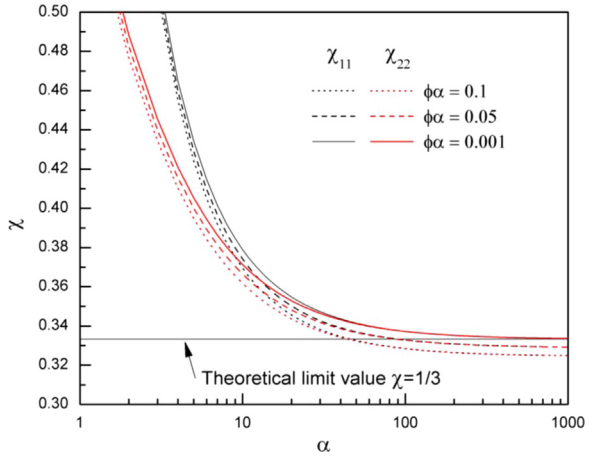

Fig. 11. Asymptotic behavior of the models for randomly-distributed high aspect ratio flakes as $\phi\alpha \to 0$.

Diffusivities $\mathcal{D}_{12}^{\sigma=20°} = \mathcal{D}_{21}^{\sigma=20°}$ are set equal to zero. These results allow us to write the diffusivity matrix in the reference configuration, $\theta = 0°$:

$$\left(\frac{\mathcal{D}}{D}\right)_{0°} = \begin{bmatrix} 0.740 & 0 \\ 0 & 0.221 \end{bmatrix}. \tag{29}$$

It is worth to mention that, for this example, there is no practical difference in estimating $(\mathcal{D}_{11}/D)_{0°}$ either with Eq. (26) or Eq. (27), since for high aspect-ratio flakes, $\alpha = 50$, the two predictions are coincident (see Fig. 9). On the other hand, if Voigt's model had been used, $(\mathcal{D}_{11}/D)_{0°} = (\mathcal{D}_{11}/D)_{Voigt}$=0.97 would had been overestimated in nearly 30% with respect to that of Eq. (27). In turn, this difference would have led to the systematic overestimation of every diffusivity component when the flake mean orientation angle is accounted for via Eq. (4) . This is illustrated in Fig. 12, which shows the evolution of the diffusivity matrix elements with $\bar{\theta}$: black curves are for $(\mathcal{D}_{11}/D)_{0°}$ given by (27) and red curves are for $(\mathcal{D}_{11}/D)_{Voigt}$.

Finally, for our case, $\bar{\theta}$=25°, the diffusivity matrix estimated by the proposed model (black curves in Fig. 12) is

$$\left(\frac{\mathcal{D}}{D}\right)_{25°} = \begin{bmatrix} 0.647 & 0.198 \\ 0.198 & 0.314 \end{bmatrix}. \tag{30}$$

9. Conclusions

A new analytical model for the prediction of the complete

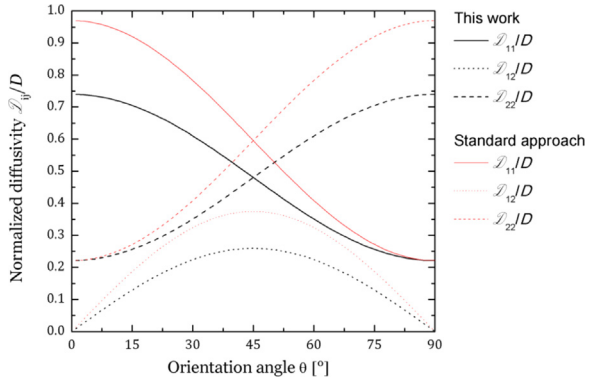

Fig. 12. Evolution of the diffusivity matrix coefficients as functions of the flake mean orientation angle. Values are for the case $\phi = 0.03$, $\alpha = 50$ and orientation dispersion $\sigma = 20°$.

diffusivity matrix of flake-filled membranes is introduced in this work. The model accounts for the effects of flake volume fraction, aspect ratio, orientation and orientational order.

The model results after the assimilation of the order parameter proposed by Bharadwaj into the model by Lape et al. Results from rigorous Boundary Element homogenization analyses are used to assess the performance and to tune the proposed model for flake volume fractions $\phi \leq 0.1$, aspect ratios $5 \leq \alpha \leq 50$ and standard normal dispersion in the orientation angle $\sigma \leq 20^{\circ}$. The model consists of a single equation for the prediction of the longitudinal and the through-the-thickness diffusivities. Complementary, it is provided a specific expression for the computation of the longitudinal diffusivities that improves the accuracy of the model for low aspect ratio flakes.

The model has been analyzed for consistency and accuracy. Model predictions for the longitudinal diffusivity are consistent to Voigt's limit for high-aspect-ratio perfectly-ordered flakes. For randomly oriented high-aspect-ratio flakes in the dilute regime, the formulas converge towards the theoretical limit by Fredrickson and Bicerano [4].

Model predictions are in very good agreement with the Boundary Element results. Predictions for through-the-thickness diffusivities deviate less than 5% from numerical results in the dilute and the intermediate regimes. Maximum discrepancies are in the concentrated regime, with differences of up to 12% for $\phi\alpha \gtrsim 2$. For the longitudinal diffusivity, discrepancies for $\phi = 0.02$ do not exceed 1%, while maximum discrepancies for $\phi = 0.05$ and $\phi = 0.1$ are 7% and 15%, respectively. They occur for the maximum flake aspect ratio and orientational disorder.

The proposed model is a versatile and useful tool for the analytical estimation of the diffusivity matrix of flake-filled membranes. The model is among the few ones that accounts for the disorder in the flake orientation, which was found to have a notorious impact on the diffusivity in the direction parallel to the flake orientation, and in turn, on the estimation of the complete diffusivity matrix when rotated at any arbitrary angle. Being analytical, the model is efficient for the implementation of optimization procedures for the multi-scale design of functionally graded materials in which flake volume fraction, aspect ratio, orientation and orientational order can be adjusted locally.

Acknowledgements

This work has been supported by grants awarded by ANPYCT (grants PICT 14-1919 and PICT 2011-0159) and the National University of Mar del Plata (grant ING 399-14).

REFERENCES

[1] N.K. Lape, E.E. Nuxoll, E.L. Cussler, Polydisperse flakes in barrier films, J. Membr. Sci. 236 (2004) 29–37.
[2] K. Wang, P. Zhao, H. Yang, S. Liang, Q. Zhang, R. Du, Q. Fu, Z. Yu, E. Chen, Unique clay orientation in the injection-molded bar of isotactic polypropylene/clay nanocomposite, Polymer 47 (2006) 7103–7110.
[3] L.E. Nielsen, Models for the permeability of filled polymer systems, J. Macromol. Sci. A 1 (1967) 929–942.
[4] G.H. Fredrickson, J. Bicerano, Barrier properties of oriented disk composites, J. Chem. Phys. 110 (4) (1999) 2181, http://dx.doi.org/10.1063/1.477829.
[5] R.K. Bharadwaj, Modeling the barrier properties of polymer-layered silicate nanocomposites, Macromolecules 34 (26) (2001) 9189–9192, http://dx.doi.org/10.1021/ma010780b.
[6] M. Fisch, S. Kumar, Introduction to liquid crystals in Liquid Crystals: Experimental Study of Physical Properties and Phase Transitons, in: S. Chandrasekhar (Ed.), 2nd ed.,Cambridge University Press, New York, 2001.
[7] L.C. Wrobel, The Boundary Element method: Applications in Thermo-fluids and Acoustics, John Wiley And Sons, 2002.
[8] Y.L. Liu, N. Nishimura, The fast multipole boundary element method for potential problems: a tutorial, Eng. Anal. Bound. Elem. 30 (5) (2006) 371–381.
[9] X. Chen, T.D. Papathanasiou, Barrier properties of flake-filled membranes: review and numerical evaluation, J. Plast. Film. Sheet. 23 (4) (2007) 319–346, http://dx.doi.org/10.1177/8756087907088437747.
[10] M. Dondero, A.P. Cisilino, J.P. Tomba, Experimental validation of computational models for mass transport through micro heterogeneous membranes, J. Membr. Sci. 437 (2013) 25–32, http://dx.doi.org/10.1016/j.memsci.2013.02.039.
[11] M. Dondero, A.P. Cisilino, J.M. Carella, J.P. Tomba, Effective thermal conductivity of functionally graded random micro-heterogeneous materials using representative volume element and BEM, Int. J. Heat. Mass Transf. 54 (2011) 3874–3881.
[12] S. Nemat-Nasser, M. Hori, Micromechanics: Overall Properties of Heterogeneous Materials, Elsevier Science, Amsterdam, 1999.
[13] W.H. Press, S.A. Teukolsky, W.T. Vetterling, B.P. Flannery, Numerical Recipes: The Art of Scientific Computing, Cambridge University Press, Cambridge, 2002.
[14] M. Minelli, M.G. Baschetti, F. Doghieri, A comprehensive model for mass transport properties in nanocomposites, J. Membr. Sci. 381 (1–2) (2011) 10–20, http://dx.doi.org/10.1016/j.memsci.2011.06.036.
[15] R. Aris, On a problem in hindered diffusion, Arch. Ration. Mech. *Anal.*. 18 (1986) 83–91.
[16] A. Greco, A. Maffezzoli, Two-dimensional and three-dimensional simulation of diffusion in nanocomposite with arbitrarily oriented lamellae, J. Membr. Sci. 442 (2013) 238–244, http://dx.doi.org/10.1016/j.memsci.2013.04.038.
[17] A. Greco, Numerical simulation and mathematical modeling of 2D multi-scale diffusion in lamellar nanocomposite, Comput. Mater. Sci. 90 (2014) 203–209, http://dx.doi.org/10.1016/j.commatsci.2014.04.017.
[18] D.M. Eitzman, R.R. Melkote, E.L. Cussler, Barrier membranes with tipped impermeable flakes, AIChE J. 42 (1) (1996) 2–9, http://dx.doi.org/10.1002/aic.690420103.
[19] H.R. Lusti, A.A. Gusev, O. Guseva, The influence of platelet disorientation on the barrier properties of composites: a numerical study, Model. Simul. Mater. Sci. Eng. 12 (2004) 1201–1207, http://dx.doi.org/10.1088/0965–0393/12/6/013.
[20] M. Dondero, A.P. Cisilino, J.P. Tomba, Numerical design of random micro-heterogeneous materials with functionally-graded effective thermal conductivities using genetic algorithms and the fast boundary element method, Comput. Model. Eng. Sci. 78 (3) (2011) 225–245.